Inorg. Chem. **2008**, *47*, 9228−9237

Theoretical Studies on the Redox Potentials of Fe Dinuclear Complexes as Models for Hydrogenase

Lindsay E. Roy, Enrique R. Batista,* and P. Jeffrey Hay

Theoretical Division, Los Alamos National Laboratory, Los Alamos, New Mexico 87545

Received March 26, 2008

Density Functional calculations have been performed at the uB3LYP and uBP86 levels to calculate the one-electron redox potentials for a series of small models based on the diiron hydrogenase enzymes in the presence of acetonitrile (MeCN). The solvation effects in MeCN are incorporated via a self-consistent reaction field (SCRF) using the polarized continuum model (PCM). The calculated redox potentials reproduce the trends in experimental data with an average error of only 0.12 V using the BP86 functional, whereas comparing results with the B3LYP functional require a systematic shift of −0.82 and −0.53 V for oxidation and reduction, respectively. The bonding orbitals and d-electron populations were examined using Mulliken population analysis, and the results were used to rationalize the calculated and observed redox potentials. These studies demonstrate that the redox potential correlates with the empirical spectrochemical series for the ligands, as well as with the amount of electron density donated by the ligand onto the Fe centers.

Introduction

Generation of molecular hydrogen has become increasingly important in recent years because of its potential as an alternate energy source.[1] One perspective in the design of inexpensive electrocatalytic materials has been provided by the hydrogenase metalloenzymes, a class of enzymes that play a fundamental role in microbial hydrogen metabolism.[2] Hydrogenases effectively catalyze the reversible oxidation of molecular hydrogen to protons and electrons according to eq 1:[3−5]

$$H_2 \rightleftharpoons 2H^+ + e^- \quad (1)$$

Metal-containing hydrogenases comprise three categories: [NiFe]-hydrogenases, [NiFe]H_2ase, where the active site contains nickel and iron ions; [FeFe]-hydrogenases, [FeFe]H_2ase, contain a dinuclear iron center in their active site; and recently another family of iron-containing hydrogenases [Fe]H_2ase, which is referred to as the iron−sulfur-cluster-free hydrogenase, only contains one iron active site and is found in the Hmd enzyme.[6−11] Although they are phylogenetically not related, it is remarkable that they all contain a low spin, low oxidation state iron center coordinated to CO and sulfur ligands. Of the hydrogenases, [FeFe]H_2ase enzymes principally reduce protons to produce H_2. The [FeFe]H_2ase active site, which is referred to as the H-cluster, contains a {2Fe2S} iron−sulfur cluster linked to a {4Fe4S} cubane via a cysteinyl-sulfur bridge (Scheme 1).[12,13]

The coordination environment of the {2Fe2S} subcluster contains carbonyl and cyanide ligands, and also a bridging dithiolate ligand where the identity of X is still under

* To whom correspondence should be addressed. E-mail: erb@lanl.gov.

(1) Turner, J. A. *Science* **2004**, *305*, 972–974.
(2) *Hydrogen as a Fuel: Learning from Nature*; Cammack, R., Frey, M., Robson, R., Eds.; Taylor & Francis: London, 2001; p 267.
(3) Albracht, S. P. *Biochim. Biophys. Acta* **1994**, *1188*, 167–204.
(4) Adams, M. W. W.; Mortenson, L. E.; Chen, J.-S. *Biochim. Biophys. Acta* **1980**, *594*, 105–176.
(5) Adams, M. W. W. *Biochim. Biophys. Acta* **1990**, *1020*, 115–145.
(6) Lyon, E. J.; Shima, S.; Boecher, R.; Thauer, R. K.; Grevels, F.-W.; Bill, E.; Roseboom, W.; Albracht, S. P. J. *J. Am. Chem. Soc.* **2004**, *126*, 14239–14248.
(7) Lyon, E. J.; Shima, S.; Buurman, G.; Chowdhuri, S.; Batschauer, A.; Steinbach, K.; Thauer, R. K. *Eur. J. Biochem.* **2004**, *271*, 195–204.
(8) Korbas, M.; Vogt, S.; Meyer.Klaucke, W.; Bill, E.; Lyon, E. J.; Thauer, R. K.; Shima, S. *J. Biol. Chem.* **2006**, *281*, 30804–30813.
(9) Pilak, O.; Mamat, B.; Vogt, S.; Hagemeier, C. H.; Thauer, R. K.; Shima, S.; Vonrhein, C.; Warkentin, E.; Ermler, U. *J. Mol. Biol.* **2006**, *358*, 798–809.
(10) Shima, S.; Thauer, R. K. *Chem. Rec.* **2007**, *7*, 37–46.
(11) Vogt, S.; Lyon, E. J.; Shima, S.; Thauer, R. K. *J. Biol. Inorg. Chem.* **2008**, *13*, 97–106.
(12) Nicolet, Y.; Piras, C.; Legrand, P.; Hatchikian, C. E.; Fontecilla-Camps, J. C. *Structure* **1999**, *7*, 13–23.
(13) Peters, J. W.; Lanzilotta, W. N.; Lemon, B. J.; Seefeldt, L. C. *Science* **1998**, *282*, 1853–1858.

10.1021/ic800541w CCC: $40.75
Published on Web 09/24/2008

Scheme 1. H-Cluster in [FeFe]H_2ase

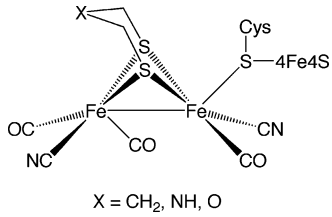

Scheme 2. Model Complex of {2Fe2S} Subcluster, [(μ-S(CH_2)$_3$S)Fe_2(CO)$_6$] (**1a**)

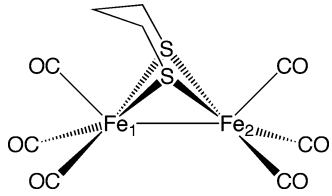

debate.[14] The iron ion distal to the {4Fe4S} cluster forms a square pyramid geometry where the open site is thought to bind H_2 or H^+ during catalysis.[14]

The large amount of structural and electronic information of the [FeFe]H_2ase has prompted numerous efforts by experimental chemists to mimic the active center of these metalloenzymes using model complexes. Among the first compounds studied is the well-known [(μ-S(CH_2)$_3$S)Fe_2(CO)$_6$] complex (Scheme 2) which has a close similarity to the {2Fe2S} moiety.[15−17]

Work by Darensbourg, Pickett, Rauchfuss, and others have examined the effects of replacing CO by more donating ligands such as cyanide, phosphines, and isocyanides as well as the role of dithiolates on the structural chemistry.[18−30] Remarkably, these compounds have been shown to exhibit electrocatalytic proton reduction.[27,31,32] The reaction pathway could involve protonation of the Fe_2 bond and, depending on the ligand, this will occur either before or after a one-electron reduction process. More recently, Rauchfuss showed that protonation at the terminal site allows for the terminal hydride to be more easily reduced than the isomeric bridging hydride.[33] In an attempt to elucidate further this proposed mechanism, De Gioia, Hall, and co-workers have conducted extensive density functional theory (DFT) studies on the reaction scheme for the dihydrogen-evolving processes described experimentally.[27,34−42]

In the case of the iron hydrogenase models, one-electron reduction potentials appear to be the driving force for electrocatalytic proton reduction. More recently in the literature, research has focused on achieving mixed valence $Fe^{II}Fe^{I}$ species which mimic the active site of the enzyme.[22,26,43−45] In an effort to assess the ability for quantitative predictions of redox potentials as well as the effects of varying the electron-donating properties of the ligands, we have undertaken a DFT investigation of a series of dinuclear Fe complexes. The standard redox potential is a fundamental chemical property which help chemists to understand many factors of a molecule including thermodynamic stability and chemical reactivity.[46] Accurate theoretical calculations in solution phase allow one to identify the electronic properties that control redox potentials on the molecular level and can be particularly useful when designing a molecule with specific redox properties *in silico*.[38,47−49]

In this paper, we examine the redox potential of a series of small molecules based on the diiron hydrogenase enzymes as calculated in the presence of solvent. Most of the

(14) Nicolet, Y.; de Lacey, A. L.; Vernede, X.; Fernandez, V. M.; Hatchikian, E. C.; Fontecilla-Camps, J. C. *J. Am. Chem. Soc.* **2001**, *123*, 1596–1601.
(15) Seyferth, D.; Henderson, R. S.; Song, L.-C. *J. Organomet. Chem.* **1980**, *192*, C1−C5.
(16) Winter, A.; Zsolnai, L.; Huttner, G. *Z. Naturforsch., B: Chem. Sci.* **1982**, *37B*, 1430–6.
(17) Lyon, E. J.; Georgakaki, I. P.; Reibenspies, J. H.; Darensbourg, M. Y. *Angew. Chem., Int. Ed.* **1999**, *38*, 3178–3180.
(18) Le Cloirec, A.; Davies, S. C.; Evans, D. J.; Hughes, D. L.; Pickett, C. J.; Best, S. P.; Borg, S. *Chem. Commun.* **1999**, 2285–2286.
(19) Lyon, E. J.; Georgakaki, I. P.; Reibenspies, J. H.; Darensbourg, M. Y. *J. Am. Chem. Soc.* **2001**, *123*, 3268–3278.
(20) Schmidt, M.; Contakes, S. M.; Rauchfuss, T. B. *J. Am. Chem. Soc.* **1999**, *121*, 9736–9737.
(21) Gloaguen, F.; Lawrence, J. D.; Schmidt, M.; Wilson, S. R.; Rauchfuss, T. B. *J. Am. Chem. Soc.* **2001**, *123*, 12518–12527.
(22) Boyke, C. A.; Rauchfuss, T. B.; Wilson, S. R.; Rohmer, M.-M.; Benard, M. *J. Am. Chem. Soc.* **2004**, *126*, 15151–15160.
(23) Zhao, X.; Georgakaki, I. P.; Miller, M. L.; Mejia-Rodriguez, R.; Chiang, C.-Y.; Darensbourg, M. Y. *Inorg. Chem.* **2002**, *41*, 3917–3928.
(24) Nehring, J. L.; Heinekey, D. M. *Inorg. Chem.* **2003**, *42*, 4288–4292.
(25) Li, P.; Wang, M.; He, C.; Li, G.; Liu, X.; Chen, C.; Akermark, B.; Sun, L. *Eur. J. Inorg. Chem.* **2005**, *250*, 6–2513.
(26) Liu, T.; Darensbourg, M. Y. *J. Am. Chem. Soc.* **2007**, *129*, 7008–7009.
(27) Tard, C.; Liu, X.; Ibrahim, S. K.; Bruschi, M.; De.Gioia, L.; Davies, S. C.; Yang, X.; Wang, L.-S.; Sawers, G.; Pickett, C. J. *Nature* **2005**, *433*, 610–613.
(28) Tard, C.; Liu, X.; Hughes, D. L.; Pickett, C. J. *Chem. Commun.* **2005**, 133–135.
(29) Best, S. P.; Borg, S. J.; White, J. M.; Razavet, M.; Pickett, C. J. *Chem. Commun.* **2007**, 4348–4350.
(30) Cheah, M. H.; Tard, C.; Borg, S. J.; Liu, X.; Ibrahim, S. K.; Pickett, C. J.; Best, S. P. *J. Am. Chem. Soc.* **2007**, *129*, 11085–11092.
(31) Borg, S. J.; Behrsing, T.; Best, S. P.; Razavet, M.; Liu, X.; Pickett, C. J. *J. Am. Chem. Soc.* **2004**, *126*, 16988–16999.
(32) Borg, S. J.; Bondin, M. I.; Best, S. P.; Razavet, M.; Liu, X.; Pickett, C. J. *Biochem. Soc. Trans.* **2005**, *33*, 3–6.
(33) Barton, B. E.; Rauchfuss, T. B. *Inorg. Chem.* **2008**, *47*, 2261–2263.
(34) Bruschi, M.; Fantucci, P.; De Gioia, L. *Inorg. Chem.* **2002**, *41*, 1421–1429.
(35) Bruschi, M.; Fantucci, P.; De Gioia, L. *Inorg. Chem.* **2003**, *42*, 4773–4781.
(36) Bruschi, M.; Zampella, G.; Fantucci, P.; De Gioia, L. *Coord. Chem. Rev.* **2005**, *249*, 1620–1640.
(37) Zampella, G.; Bruschi, M.; Fantucci, P.; Razavet, M.; Pickett, C. J.; De.Gioia, L. *Chem.—Eur. J.* **2005**, *11*, 509–520.
(38) Greco, C.; Zampella, G.; Bertini, L.; Bruschi, M.; Fantucci, P.; De.Gioia, L. *Inorg. Chem.* **2007**, *46*, 108–116.
(39) Cao, Z.; Hall, M. B. *J. Am. Chem. Soc.* **2001**, *123*, 3734–3742.
(40) Fan, H.-J.; Hall, M. B. *J. Am. Chem. Soc.* **2001**, *123*, 3828–3829.
(41) Tye, J. W.; Darensbourg, M. Y.; Hall, M. B. *J. Comput. Chem.* **2006**, *27*, 1454–1462.
(42) Borg, S. J.; Tye, J. W.; Hall, M. B.; Best, S. P. *Inorg. Chem.* **2007**, *46*, 384–394.
(43) Boyke, C. A.; van der Vlugt, J. I.; Rauchfuss, T. B.; Wilson, S. R.; Zampella, G.; De Gioia, L. *J. Am. Chem. Soc.* **2005**, *127*, 11010–11018.
(44) Justice, A. K.; Rauchfuss, T. B.; Wilson, S. R. *Angew. Chem., Int. Ed.* **2007**, *46*, 6152–6154, S6152/1−S6152/27.
(45) Justice, A. K.; Nilges, M. J.; Rauchfuss, T. B.; Wilson, S. R.; De Gioia, L.; Zampella, G. *J. Am. Chem. Soc.* **2008**, *130*, 5293–5301.
(46) Bard, A. J.; Faulkner, L. R. *Electrochemical Methods: Fundamentals and Applications*; Wiley: New York, 1980; p 718.
(47) Baik, M.-H.; Friesner, R. A. *J. Phys. Chem. A* **2002**, *106*, 7407–7412.
(48) Holland, J. P.; Green, J. C.; Dilworth, J. R. *Dalton Trans.* **2006**, 783–794.
(49) Jaque, P.; Marenich, A. V.; Cramer, C. J.; Truhlar, D. G. *J. Phys. Chem. C* **2007**, *111*, 5783–5799.

compounds chosen have been extensively characterized by a variety of methods including X-ray crystallography, IR spectroscopy, and cyclic voltammetry. Since many of the compounds have been validated by DFT methods in the past, we will only discuss our calculated structures and experimental data when necessary. Instead, our focus will be on the calculated redox potentials and how they relate to the experiment. These studies demonstrate how the redox potential correlates with the empirical spectrochemical series for the ligands as well as with the amount of electron density donated by the ligand onto the Fe centers.

Computational Details and Theoretical Background

Density Functional Calculations. All calculations were carried out using Gaussian 03 (E.01 Version).[50] Geometry optimizations of the gas-phase compounds for all oxidation states were performed using two DFT methods. The first functional is the generalized gradient approximation (GGA) functional BP86 which combines Becke's 1988 exchange functional (B) with Perdew's 1986 (P86) correlation functional.[51,52] The second approach is the hybrid B3LYP method, which incorporates Becke's three-parameter exchange functional (B3) with the Lee, Yang, and Parr (LYP) correlation functional.[53,54] The effective core potential and associated basis set of Hay and Wadt LANL2DZ[55,56] with optimized diffuse and polarization functions (LANL2DZdp)[57] for sulfur and phosphorus, and modified Couty-Hall LANL2DZ[58] basis set was used for iron. The 6−31G** basis set was used for carbon, nitrogen, and hydrogen atoms of the μ-SRS linkers, and all other atoms use the 6−311G* triple-ζ with polarization basis set. All geometries were optimized without constraints and verified by vibrational analyses at the same level of theory to ensure that they correspond to minima on the potential energy surface. The vibrational frequencies were unscaled for the BP86 functional and scaled by a factor of 0.9569 to reproduce the harmonic frequencies for B3LYP. These frequencies then derived the zero-point-energy (ZPE) and electronic, vibrational, and rotational corrections at 298.15 K. The spin-unrestricted approach was employed for all calculations, and we assumed a low-spin Fe complex in all cases.

Scheme 3. Born−Haber Cycle

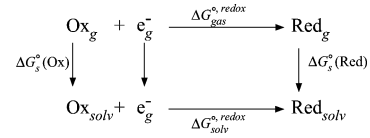

Solvation Free Energies and Calculations of Redox Potentials. The solvation free energies, ΔG°_s, for the complexes in all oxidation states were evaluated by the self-consistent reaction field (SCRF) approach based on the polarized continuum model (PCM) level of theory using the gas-phase geometries.[59] In PCM, the solvent is represented by a polarized dielectric medium characterized by the relative dielectric constant of the bulk, and a set of optimized radii are used to build an effective cavity occupied by the solute in the solvent. The solute−solvent boundary has been derived using a solvent excluding surface (SES).[60] This is the surface traced by the solvent sphere as it rolls over the molecular surface of the solute defined using the United Atom Universal Force Field topological model (UFF) for the radii of the solute atoms.[61] All SCRF calculations were performed with the default options implemented in Gaussian 03. Acetonitrile (MeCN) solvent model was employed with a dielectric constant of 36.64, and the sphere radius of the solvent (R_{solv}) is 2.155 Å. The choice of solvent was based on the solvent medium for all electrochemistry experiments used to compare with the calculations. For the solute interior, a dielectric constant of 1.0 is used throughout.

To determine the redox potentials, the free energy change of the half-reactions is represented by the thermodynamic (Born−Haber) cycle as shown in Scheme 3;[62] in terms of the free energy change in the gas phase, $\Delta G_g^{\circ,redox}$, and the solvation free energies of the oxidized, ΔG°_s(Ox), and reduced, ΔG°_s(Red), species. The overall reaction (eq 2) is characterized by the standard Gibbs free energy, $\Delta G_{solv}^{\circ,redox}$/kcal·mol^{-1};

$$\Delta G^{\circ,redox}_{solv} = \Delta G^{\circ,redox}_{g} + \Delta G^{\circ}_s(\mathrm{Red}) - \Delta G^{\circ}_s(\mathrm{Ox}) \qquad (2)$$

and the standard one-electron redox potentials, E°/V, is calculated using the Nernst eq 3;

$$\Delta G^{\circ,redox}_{solv} = -FE^{\circ}_{calc} \qquad (3)$$

where F is the Faraday constant, 23.06 kcal mol^{-1} V^{-1}. The free energy change in the gas phase, $\Delta G_g^{\circ,redox}$, can be easily derived following eqs 4 and 5, where ε is the energy.

$$\Delta H^{\circ,redox}_{g} = \mathrm{d}\varepsilon_{SCF} + \mathrm{d}\varepsilon_{trans} + \mathrm{d}\varepsilon_{rot} + \mathrm{d}\varepsilon_{vib} + \mathrm{d}\varepsilon_{ZPE} \qquad (4)$$

$$\Delta G^{\circ,redox}_{g} = \Delta H^{\circ,redox}_{g} - T\Delta S^{\circ,redox}_{g} \qquad (5)$$

All terms in eqs 2−5 are at 298.15 K except $\mathrm{d}\varepsilon_{SCF}$ which is at 0 K. The solvation free energy, ΔG°_s is partitioned into two contributions (eq 6):[49]

$$\Delta G^{\circ}_s = \Delta G_{EE} + \Delta G_{CDR} \qquad (6)$$

The first term accounts for the bulk electrostatic effects (EE) including the energy difference between the solute polarized by

(50) Frisch, M. J.; Trucks, G. W.; Schlegel, H. B.; Scuseria, G. E.; Robb, M. A.; Cheeseman, J. R. ; Montgomery J.A., Jr.; Vreven, T.; Kudin, K. N.; Burant, J.C.; Millam, J. M.; Iyengar, S. S.; Tomasi, J.; Barone, V.; Mennucci, B.; Cossi, M.; Scalmani, G.; Rega, N.; Petersson, G. A.; Nakatsuji, H.; Hada, M.; Ehara, M.; Toyota, K.; Fukuda, R.; Hasegawa, J.; Ishida, M.; Nakajima, T.; Honda, Y.; Kitao, O.; Nakai, H.; Klene, M.; Li, X.; Knox, J. E.; Hratchian, H. P.; Cross, J. B.; Bakken, V.; Adamo, C.; Jaramillo, J.; Gomperts, R.; Stratmann, R. E.; Yazyev, O.; Austin, A. J.; Cammi, R.; Pomelli, C.; Ochterski, J. W.; Ayala, P. Y.; Morokuma, K.; Voth, G. A.; Salvador, P.; Dannenberg, J. J.; Zakrzewski, V. G.; Dapprich, S.; Daniels, A. D.; Strain, M. C.; Farkas, O.; Malick, D. K.; Rabuck, A. D.; Raghavachari, K.; Foresman, J. B.; Ortiz, J. V.; Cui, Q.; Baboul, A. G.; Clifford, S.; Cioslowski, J.; Stefanov, B. B.; Liu, G.; Liashenko, A.; Piskorz, P.; Komaromi, I.; Martin, R. L.; Fox, D. J.; Keith, T.; Al.Laham, M. A.; Peng, C. Y.; Nanayakkara, A.; Challacombe, M.; Gill, P. M. W.; Johnson, B.; Chen, W.; Wong, M. W.; Gonzalez, C.; Pople, J. A. *Gaussian 03*; Gaussian, Inc.: Wallingford, CT, 2004.
(51) Becke, A. D. *Phys. Rev. A: At., Mol., Opt. Phys.* **1988**, *38*, 3098–3100.
(52) Perdew, J. P. *Phys. Rev. B* **1986**, *33*, 8822.
(53) Becke, A. D. *J. Chem. Phys.* **1993**, *98*, 5648–5652.
(54) Lee, C.; Yang, W.; Parr, R. G. *Phys. Rev. B* **1988**, *37*, 785–789.
(55) Hay, P. J.; Wadt, W. R. *J. Chem. Phys.* **1985**, *82*, 270–283.
(56) Wadt, W. R.; Hay, P. J. *J. Chem. Phys.* **1985**, *82*, 284–298.
(57) Check, C. E.; Faust, T. O.; Bailey, J. M.; Wright, B. J.; Gilbert, T. M.; Sunderlin, L. S. *J. Phys. Chem. A* **2001**, *105*, 8111–8116.
(58) Couty, M.; Hall, M. B. *J. Comput. Chem.* **1996**, *17*, 1359–1370.
(59) Cossi, M.; Scalmani, G.; Rega, N.; Barone, V. *J. Chem. Phys.* **2002**, *117*, 43–54.
(60) Connolly, M. L. *Science* **1983**, *221*, 709–713.
(61) Rappe, A. K.; Casewit, C. J.; Colwell, K. S.; Goddard, W. A., III; Skiff, W. M. *J. Am. Chem. Soc.* **1992**, *114*, 10024–10035.
(62) Li, J.; Fisher, C. L.; Chen, J. L.; Bashford, D.; Noodleman, L. *Inorg. Chem.* **1996**, *35*, 4694–4702.

the reaction field of the solvent minus the nonpolarized, *in vacuo* solute energy. The second term accounts for the sum of the cavitation and the dispersion-repulsion energies (CDR).

We considered including a geometry relaxation energy, $d\varepsilon_{geom}$, obtained by fully optimizing $[(\mu\text{-}S(CH_2)_3S)Fe_2(CO)_6]$ (**1a**) with solvent effects. Comparing the electronic energy values of the fully optimized compound with solvent effects and the single point calculation using the optimized *in vacuo* structure, the energy of **1a** was found to be 0.23 and 0.74 kcal mol^{-1} for the Fe^IFe^I and Fe^0Fe^I complexes, respectively. For the thermodynamic cycle, this results in an overall change in the geometry relaxation energy, $dd\varepsilon_{geom}$, of 0.51 kcal mol^{-1}. The contribution to the potential is only a small perturbation of ~0.02 V, and the computational cost outweighs the improved accuracy in the potential.

When calculating the oxidation potential of the Fe^IFe^I species, in actuality we are calculating the reduction potential of the $Fe^{II}Fe^I$ complexes following the Born−Haber cycle (Scheme 3), and the values in the text are $-E^\circ_{calc}$ of the $Fe^{II}Fe^I|Fe^IFe^I$ reduction potential. Also, the computed absolute potential, E°_{calc}, is not referenced to any standard electrode. We chose to reference our computed potentials to ferrocene (Fc), and the absolute half-cell $Fc^+|Fc$ couple was computed to be −4.95 V (−5.28 V) using BP86 (B3LYP). We employed the same modified LANL2dz basis set for iron and 6−311G* basis set for carbon and hydrogen. In addition, all experimental potentials are reported versus Fc. Note that 0.0 V versus Fc/Fc^+ = 0.087 V versus 0.01 M $Ag/AgNO_3$ = 0.38 V versus SCE = 0.425 V versus sat. Ag/AgCl = 0.630 V versus NHE in MeCN at 25 °C.[63]

Results and Discussion

Before our discussion of the one-electron redox potentials for the series, we will first compare our optimization results to experiment. Then, upon introducing the calculated redox potentials, our discussion will focus on how the various donor ligands affect the observed redox properties.

Molecular Structures. To assess the initial accuracy of our calculations in modeling the complexes, the optimized geometries for a series of $(\mu\text{-SRS})[Fe(CO)_2L]_2$ species were compared to the experimental structures derived from X-ray crystallography (Figure 1).[21,25,64−68] As has been shown previously, the DFT calculation with the uB3LYP and uBP86 method show excellent agreement with experiment.[22,34−37,39,40,68,69] However, since our latter discussion will depend on accurate calculations of thermodynamic cycles, it is important for us to first confirm our methodology by comparing our optimization results to experimental data, whenever possible.

Comparison between the optimized geometries and those complexes which have X-ray crystallographic data show that

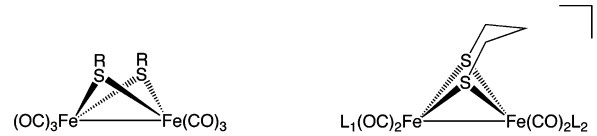

1a: $(SR)_2 = S(CH_2)_3S$
b: $(SR)_2 = S(CH_2)_2S$
c: SR = SEt
d: $(SR)_2 = SCH_2C_6H_4CH_2S$
e: $(SR)_2 = SCH_2N(Ph)CH_2S$
f: $(SR)_2 = SCH_2N(CH_2Ph)CH_2S$

2a: $L_1 = CO, L_2 = CNCH_3, n = 0$
b: $L_1 = CO, L_2 = PPh_3, n = 0$
c: $L_1 = CO, L_2 = PPh(CH_3)_2, n = 0$
d: $L_1 = L_2 = CNCH_3, n = 0$
e: $L_1 = L_2 = PPh(CH_3)_2, n = 0$
f: $L_1 = L_2 = CN, n = 2-$

Figure 1. Structures for a series of synthetic models for the active site of $[FeFe]H_2$ase.

the greatest variance lies in the metal−ligand bonds; the Fe−S bonds are consistently overestimated in all complexes by 0.04−0.09 Å, and the Fe−C distances differ by 0.01−0.04 Å using both functionals. The largest variance can be found in complex **2f**, which is not surprising given its anionic charge.[70] However, these values still lie within the standard deviation for the B3LYP and BP86 functionals.[71] The calculated vibrational stretching frequencies for the ν(CO) and ν(CN) bands were compared versus experiment. The gas phase DFT calculations yield accurate estimates of experimentally determined stretching frequencies for the series of Fe^IFe^I complexes studied. While it seems necessary to use a scaling factor when comparing harmonic frequencies obtained with the B3LYP functional, this factor is not needed for frequency calculations of large molecules using the BP86 functional because of an error cancelation effect.[41,72]

Of the compounds considered, two do not have crystal structure information, namely, **2a** and **2d**. To gain insight into the possible coordination configurations of structures **2a** and **2d** using isocyanide ligands, the proposed geometries were optimized using DFT. There are four possible isomers for mono- and disubstitution on each iron center of $(\mu\text{-}S(CH_2)_3S)[Fe(CO)_3]_2$, shown in Scheme 4. A comparison of the structures in **2a** reveals that the Fe−Fe distance is unaffected by the substitution placement and the bond distance changes by 0.008 Å, with the shorter bond distance seen in the apical (Ap1 and Ap2) isomers. The relative energy between the isomers (Ba1 and Ba2) in gas phase differs by less than 2 kcal mol^{-1}, and the lowest energy conformations, the basal isomers, are separated by only 0.02 kcal mol^{-1}. However, there does appear to be a difference in ν_{CN} stretching frequencies in the apical versus basal arrangement; both apical isomers have ν_{CN} stretches at ~2160 cm^{-1} while the basal isomers show a stretching frequency at ~2178 cm^{-1} (bp86). IR spectral data only features one band at 2185 cm^{-1} for ν_{CN} with no mention of a shoulder.[21] Perhaps the line broadening brought on by the polarity of the solvent might mask the double peak structure. When considering solvent effects, we found that the solvent stabilizes the isomers further, and the relative energy difference decreases to <0.61 kcal mol^{-1}, which is on the order of kT at room temperature. Because of possible conformational flexibility, all isomers of **2a** may be present

(63) Pavlishchuk, V. V.; Addison, A. W. *Inorg. Chim. Acta* **2000**, *298*, 97–102.
(64) Chong, D.; Georgakaki, I. P.; Mejia-Rodriguez, R.; Sanabria-Chinchilla, J.; Soriaga, M. P.; Darensbourg, M. Y. *Dalton Trans.* **2003**, 4158–4163.
(65) Ott, S.; Kritikos, M.; Akermark, B.; Sun, L.; Lomoth, R. *Angew. Chem., Int. Ed.* **2004**, *43*, 1006–1009.
(66) Capon, J.-F.; Gloaguen, F.; Schollhammer, P.; Talarmin, J. *Coord. Chem. Rev.* **2005**, *249*, 1664–1676.
(67) Ekstroem, J.; Abrahamsson, M.; Olson, C.; Bergquist, J.; Kaynak, F. B.; Eriksson, L.; Sun, L.; Becker, H.-C.; Aakermark, B.; Hammarstroem, L.; Ott, S. *Dalton Trans.* **2006**, 4599–4606.
(68) Hou, J.; Peng, X.; Liu, J.; Gao, Y.; Zhao, X.; Gao, S.; Han, K. *Eur. J. Inorg. Chem.* **2006**, 4679–4686.
(69) Liu, Z.-P.; Hu, P. *J. Am. Chem. Soc.* **2002**, *124*, 5175–5182.
(70) Petrie, S.; Stranger, R. *Inorg. Chem.* **2004**, *43*, 2597–2610.
(71) Buehl, M.; Kabrede, H. *J. Chem. Theory Comput.* **2006**, *2*, 1282–1290.
(72) Neugebauer, J.; Hess, B. A. *J. Chem. Phys.* **2003**, *118*, 7215–7225.

Scheme 4. Possible Mono- and Disubstituted Isomers for **2a** and **2d**

Monosubstituted:

Ap1 Ba1 Ba2 Ap2

Disubstituted:

Ap/Ap Ap/Ba transoid Ba/Ba cisoid Ba/Ba

Table 1. Computed Relative Stabilities of Isomers for Compounds **2a** and **2d**

	relative gas phase energies (kcal mol^{-1})		relative solvent energies (kcal mol^{-1})	
compound	BP86	B3LYP	BP86	B3LYP
2a-Ap1	1.60	1.60	0.42	0.12
2a-Bas1	0.02	0.12	0.00	0.32
2a-Bas2	0.00	0.00	0.01	0.00
2a-Ap2	1.73	1.67	0.61	0.44
2d-Ap/Ap	10.81	10.24	10.05	13.77
2d-Ba/Ba-trans	2.23	1.92	3.75	3.85
2d-Ba/Ba-cis	0.00	0.00	0.00	0.00
2d-Ap/Ba	3.82	3.46	4.25	4.07

in solution and will therefore be included in our analysis of reduction potentials.

For the displacement of two carbonyl ligands, all four conformations can be related to one or two well characterized examples in the literature.[20,23−25,68,73] X-ray structure analysis for complexes such as (μ-S(CH$_2$)$_3$S)[Fe(CO)$_2$PMe$_3$]$_2$ possess a transoid Ba/Ba arrangement.[23] In contrast, PMe$_2$Ph- and *t*BuNC-disubstituted complexes show a preference for Ap/Ap coordination, presumably because of the steric requirements of the ligands.[24,25] It is also important to point out that complexes such as (μ-S(CH$_2$)$_3$S)[Fe(CO)$_2$CN]$_2^{2-}$ and (μ-SCH$_2$N(R)CH$_2$S)$_3$S)[Fe(CO)$_2$(4-IC$_6$H$_4$NC)]$_2$ adopt an Ap/Ba and cisoid Ba/Ba configuration, respectively, implying that both steric and electronic effects of a ligand control the stereochemistry.[20,68] Interestingly, geometry optimizations of the four isomers of **2d** reveal that the lowest energy solution possesses the cisoid Ba/Ba configuration (Table 1). The transoid Ba/Ba arrangement is ~2 kcal mol^{-1} higher in energy, and the energy difference between all isomers is less than 10 kcal mol^{-1} of each other. We find that when including solvent effects, the relative stabilization sequence does not change and the cisoid Ba/Ba configuration is still preferred. As is the case with **2a**, all of the isomers calculated also have an additional ν_{CN} stretch at lower frequencies than reported. However, there could be an indication of isomerism in the ν_{CO} bands; only one isomer (Ap/Ap) has a ν_{CO} stretching frequency close to the experimental peak of ~2020 cm^{-1}.[21] Although there is some indication that all isomers could be present in the experiment, we will only consider the cisoid and transoid Ba/Ba configurations because of the larger energy separation between isomers compared to **2a**.

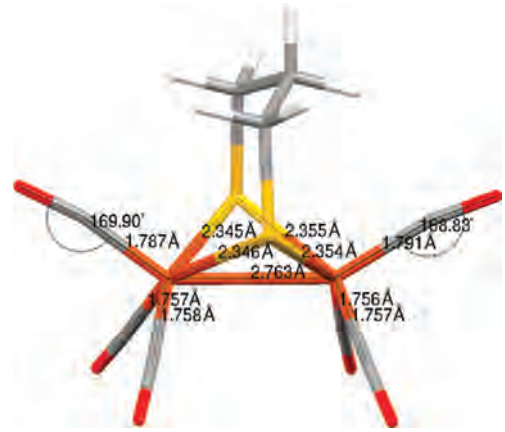

Figure 2. Optimized structure for [**1a**]$^-$.

The optimized structure of the reduced analogue for species **1a** is shown in Figure 2. In addition to a longer Fe−Fe distance compared to the neutral complex, the reduced analogues all exhibit a characteristic bend of the apical carbonyl ligands of ~10° along Fe−C−O angle upon addition of an electron to the neutral species. The reduced species of **1a** and **1b** have been previously characterized using IR spectroscopy and DFT calculations by Best, Hall, and co-workers.[42] The calculated IR spectra for the two compounds are indistinguishable in the ν_{CO} region and are expected to have similar structures to that of the neutral analogue. The calculated IR spectra for [**1a**]$^-$ and [**1b**]$^-$ using the BP86 functional are presented in the Supporting Information, and the results are very similar to the experimental ones. The same type of Fe−C−O bending seen in [**1a**]$^-$ also occurs for the methylisocyanide ligand regardless of its coordination environment to the Fe centers. Shown in the Supporting Information, Figure S6, complexes [**2a**]$^-$ and [**2d**]$^-$ exhibit a ~40° bend of the C−N−CH$_3$ angle from typical 180° for an isocyanide ligand. However, no bend or distortion occurs among the phosphine or cyanide ligands.

Modeling the mixed-valence Fe^{II}Fe^{I} oxidation state is more of a challenge because of the difficulty in isolating and characterizing the complexes. Recent reports in the literature

(73) Mejia-Rodriguez, R.; Chong, D.; Reibenspies, J. H.; Soriaga, M. P.; Darensbourg, M. Y. *J. Am. Chem. Soc.* **2004**, *126*, 12004–12014.

Figure 3. Three possible isomers for the mixed-valence $Fe^{II}Fe^{I}$ state. Complex $[\mathbf{1a}]^+$ is shown as an example.

show that more "electron-rich" Fe_2 species with phosphines, isocyanides, or N-heterocyclic carbene are able to stabilize a mixed valence $Fe^{II}Fe^{I}$ or diferrous state of the complex.[22,26,43−45] The mixed valence state of the complexes exist as an entatic state or "rotated" structure resembling the enzyme with a semibridging CO and a protected open site. In modeling the aforementioned complexes, we wanted to ensure that we were obtaining the correct ground-state for each species. There are three possible isomers, shown in Figure 3, depending on the nature of the carbonyl ligands: Ox1 closely resembles that of the neutral form of the complexes, Ox2 has a "rotated" structure which contains a semibridging CO ligand and the open Fe site is protected by the bridging dithiolate ligand, and Ox3 is also a "rotated" structure, but the open site is not protected by the dithiolate. Note that complexes $[\mathbf{1b}]^+$, $[\mathbf{1c}]^+$, and $[\mathbf{2e}]^+$ exist as only two isomers, Ox1 and Ox2.

We were able to optimize all of the isomers for the mono- and disubstituted complexes with a few exceptions; the Ox1 starting structure of the phosphine-substituted compounds of **2b**, **2c**, and **2e** all converged to the Ox2 structure. For the hexacarbonyl dithiolate analogues, we were only able to optimize the Ox3 structure for **1a** and **1d**. As has been shown with the more electron-rich $Fe^{II}Fe^{I}$ compounds, Ox2 was found to be the most favorable isomer of all the species with an average energy difference of ∼4 kcal mol^{-1} for Ox1. Surprisingly, Ox2 and Ox3 geometries differ by less than 1 kcal mol^{-1} in most cases, with a transition state between Ox2 and Ox3 for complex $[\mathbf{1a}]^+$ that is at ∼5 kcal mol^{-1} for both functionals. While both isomers are more than likely present during redox experiments, our calculations will only focus on the Ox2 isomer since the energy difference is nominal.

Another scenario that could occur in these oxidized complexes is having a bridging or semibridging cyanide/isocyanide group; PMe_2Ph- and PPh_3- derivatives are excluded because of the steric requirements of the ligands. Bénard, Rauchfuss, and co-workers discussed in detail the bonding and electronic structure aspects of a bridging CO versus CNMe ligand in a diferrous species.[22] Our calculations predict that a μ-CN or μ-CNMe ligand is less stable than the μ-CO forms by 11 and 5 kcal mol^{-1}, respectively. Therefore, it is unlikely that a μ-CN or μ-CNMe complex is present in the experimental redox studies, and we will only concern ourselves with a μ-CO bridging ligand in complexes **2a**, **2d**, and **2f**.

Table 2. One-Electron Oxidation and Reduction Potentials of the $Fe^{I}Fe^{I}$ Complexes Studied in This Investigation[a]

	$E°$/V (expt)		$E°$/V (calc, BP86)		$E°$/V (calc, B3LYP)		
complex	Ox	Red	Ox	Red	Ox	Red	ref
1a	0.78[b]	−1.59	0.96	−1.59	0.10	−1.98	21
1b	0.93[c]	−1.54	1.10	−1.56	0.24	−2.08	64
1c	0.82[c]	−1.55	0.65	−1.51	−0.11	−1.87	64
1d	0.84[c]	−1.41	0.83	−1.45	0.13	−1.90	64
1e	0.55[d]	−1.55	0.50	−1.50	−0.11	−1.97	68
1f		−1.56[d]	0.45	−1.49	−0.17	−2.05	65
2a-Ap1	0.59[b]	−1.79	0.60	−2.14	−0.25	−2.40	21
2a-Ba1	0.59[b]	−1.79	0.63	−1.89	−0.27	−2.32	21
2a-Ba2	0.59[b]	−1.79	0.54	−1.90	−0.27	−2.33	21
2a-Ap2	0.59[b]	−1.79	0.62	−2.00	−0.26	−2.31	21
2b	0.26[e]	−1.85	0.28	−1.83	−0.46	−2.17	25
2c	0.25[e]	−1.91	0.26	−1.95	−0.73	−2.32	25
2d-Ba/Ba-trans	0.23[b]	−2.18	0.25	−2.22	−0.70	−2.77	21
2d-Ba/Ba-cis	0.23[b]	−2.18	0.27	−2.15	−0.74	−2.68	21
2e	−0.14[e]	−2.31	−0.11	−2.39	−0.54	−2.73	25
2f	−0.51[b]	−2.71	−0.75	−2.89	−1.50	−3.69	21
rms[f]			0.11	0.13	0.82	0.53	
R^2			0.94	0.88	0.72[g]	0.87[h]	

[a] All potentials are quoted against ferrocene (Fc). [b] Experimental value reported vs Ag/AgCl (sat. KCl). [c] Experimental value reported vs NHE. [d] Experimental value reported vs Fc. [e] Experimental value reported vs 0.01 M $Ag/AgNO_3$. [f] Root mean square error. [g] Based on $y = x + 0.82$. [h] Based on $y = x + 0.53$.

Calculation of One-Electron Redox Potentials. The different ligands were chosen to investigate the effects on the structure, orbitals, and calculated redox potentials of the $Fe^{I}Fe^{I}$ complexes. If the redox potentials are dependent upon the electronic nature of the ligands, then it is logical to assume that the more electron donating groups would stabilize the $Fe^{I}Fe^{I}$ complex, thereby lowering the redox potentials. Table 2 shows the calculated oxidation and reduction potential, respectively, versus experiment using the BP86 and B3LYP functionals. A more detailed breakdown on changes in the electron attachment or ionization potential *in vacuo*, with the ZPE, thermal, and entropy corrections, and the change in free energy of solvation $\Delta\Delta G°_s$ (reduced-oxidized) in acetonitrile can be found in the Supporting Information.

Figure 4 shows a plot of the calculated redox potentials for complexes **1a**−**2f** versus the experimental potentials, $E_{1/2}$/V, measured in MeCN. Linear regression analysis indicates that the quality of the fit of the calculation to experiment is very

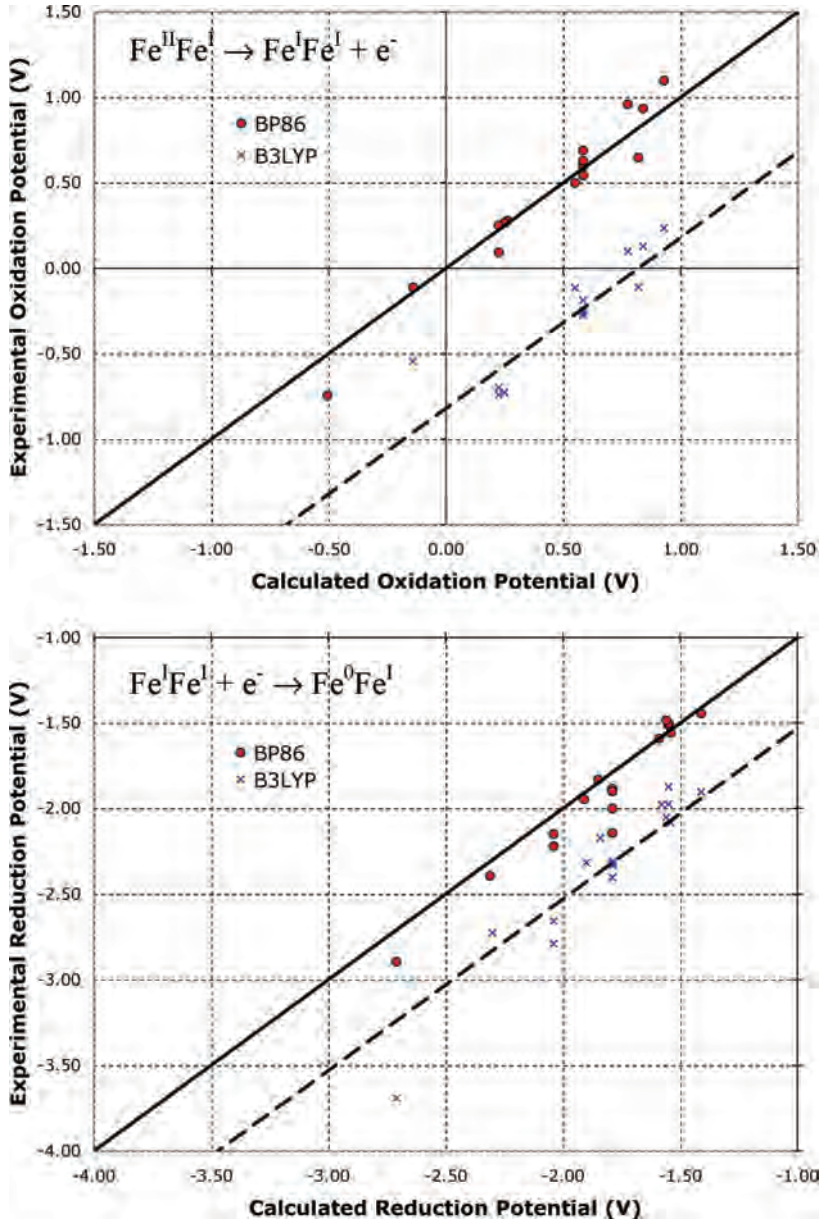

Figure 4. Correlation diagram of calculated vs experimental oxidation (top) and reduction (bottom) potentials, $E_{1/2}$ (Fc)/V for $Fe^{I}Fe^{I}$ complexes using BP86 and B3LYP functionals.

good with R^2 values of 0.94 and 0.88 for the oxidation and reduction potentials, respectively, with an average discrepancy of 0.12 V for the BP86 functional. However, a systematic error is observed when using B3LYP that gives rise to a consistent shift of −0.82 (−0.53) V for the oxidation (reduction) potential. When including the baseline shift, a fairly high correlation coefficient of 0.72 and 0.87 for oxidation and reduction potentials, respectively, was found between experiment and theory. These results were somewhat surprising in light of the moderate success of the B3LYP functional to predict the redox potential for a variety of inorganic compounds, although differences on 0.5 V were noted for Fe, Ru, and Os complexes with ligands similar to the ones studied here.[47−49,74−76] Also, the most accurate results required computationally demanding correlation-consistent triple-ζ basis sets plus a double set of diffuse functions. On the basis of our results, BP86 is a better choice of functional for correlating our results with experiment, and we will only focus on those results for the remainder of this paper.

When the different isomers of **2a** and **2d** are looked at, the lowest energy isomer best correlates with the experimental reduction potential, even though cyclic voltammetry experiments indicate that it is irreversible.[21] It is interesting to note that there is ∼100−150 meV difference between apical versus basal substitution using BP86 in complex **2a**. Also, there is almost no difference between reduction potentials of the basal substituted isomers in both **2a** and **2d**. Upon removing the higher energy isomers of **2a** and **2d**, the linear relationship improves between E_{calc} and experiment

(74) Siegbahn, P. E. M. *Adv. Inorg. Chem.* **2004**, *56*, 101–125.
(75) Yang, X.; Baik, M.-H. *J. Am. Chem. Soc.* **2004**, *126*, 13222–13223.
(76) Tsushima, S.; Wahlgren, U.; Grenthe, I. *J. Phys. Chem. A* **2006**, *110*, 9175–9182.

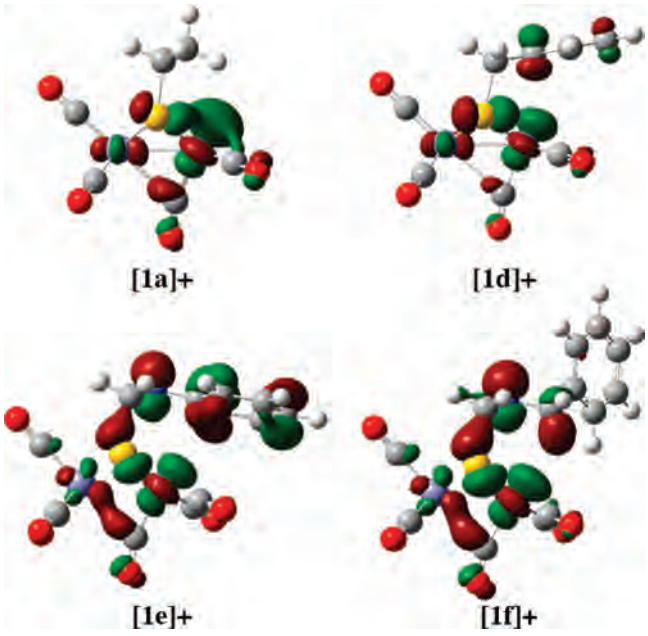

Figure 5. SOMO of $[\mathbf{1a}]^+$ (top left), $[\mathbf{1d}]^+$ (top right), $[\mathbf{1e}]^+$ (bottom left), and $[\mathbf{1f}]^+$ (bottom right).

Table 3. Derived Constants for Equation 7

	a	*b*
oxidation/$E_{Fe^IFe^IHOMO}$	−0.665	3.141
reduction/$E_{Fe^IFe^ILUMO}$	−0.705	3.957

with an average R^2 value of 0.95 with BP86. These results show that excellent agreement can be obtained using a dielectric continuum model, and that theory can accurately replicate the solvent used in cyclic voltammetry experiments.

Placing the complexes in order of calculated redox potential, E_{calc}, the trend is as follows for the neutral dinuclear complexes $[(\mu\text{-}S(CH_2)_3S)Fe_2(CO)_4(L_1)(L_2)]$: $L_1 = L_2 = CO$ (**1a**) > $L_1 = CO$, $L_2 = PPh_3$ (**2b**) > $L_1 = CO$, $L_2 = CNCH_3$ (**2a**) > $L_1 = CO$, $L_2 = PPh(CH_3)_2$ (**2c**) > $L_1 = L_2 = CNCH_3$ (**2d**) > $L_1 = L_2 = PPh(CH_3)_2$ (**2e**) > $L_1 = L_2 = CN$ (**2f**). Among the diiron hexacarbonyl dithiolate complexes, the choice of bridge (**1a**−**1f**) does not cause an appreciable shift in the reduction potential, including the basic azadithiolate bridge. The only dramatic shift occurs in complex **1d** where changing the bridge from aliphatic to aromatic causes a 0.18 V shift toward more positive potentials. This trend is expected considering that the lowest unoccupied molecular orbital (LUMO) of the Fe^IFe^I hexacarbonyl complexes contains little dithiolate bridging character (∼6.6% in **1a** and ∼7.6% in **1d**). In contrast, the oxidation potentials for the azadithiolate bridging complexes are shifted by ∼30 mV compared to other μ-dithiobis(tricarbonyliron) derivatives. To help elucidate why the azadithiolates are easier to oxidize, Figure 5 shows the singly occupied molecular orbitals (SOMO) for $[\mathbf{1a}]^+$, $[\mathbf{1d}]^+$, $[\mathbf{1e}]^+$, and $[\mathbf{1f}]^+$. From the figure, the amount of dithiolate bridging character in the SOMO of the azadithiolates is considerable (63% in $[\mathbf{1e}]^+$ and 49% in $[\mathbf{1f}]^+$) compared to their propanedithiolate counterpart (20% in $[\mathbf{1a}]^+$). Examination of the SOMO orbital of $[\mathbf{1e}]^+$ reveals that it is destabilized by two antibonding interactions; the central nitrogen bridgehead forms a π antibond with the phenyl group, and the open Fe site forms a d-π interaction with the aromatic ring. This same d-π interaction also occurs in complex $[\mathbf{1d}]^+$ but hardly changes oxidation potential compared to $[\mathbf{1a}]^+$. Therefore, the basic site at the bridge somewhat destabilizes the orbital and the π^* interaction causes a substantial shift in the oxidation potential. Similarly, the CH group from the benzyl moiety in $[\mathbf{1f}]^+$ interacts with the nitrogen bridgehead. Upon inspection of the other systems, the majority of the oxidation and reduction potentials are based on the metal−metal and metal−CO character in the Fe^IFe^I highest occupied molecular orbital (HOMO) and LUMO, respectively.

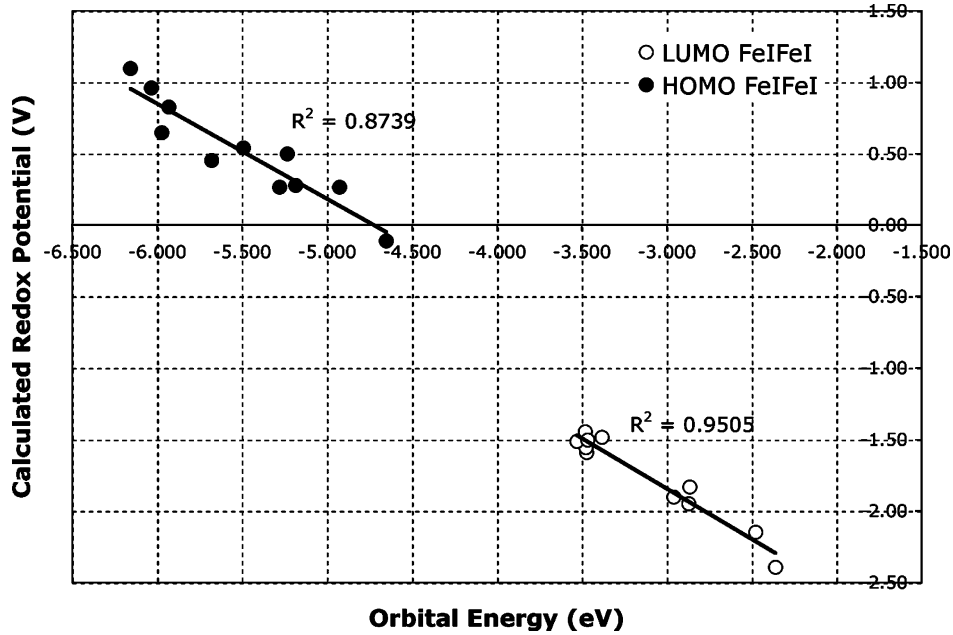

Figure 6. HOMO (closed circles) and LUMO (open circles) gas phase energies/eV of the Fe^IFe^I complexes vs the calculated redox potentials, E_{calc}/V, using the BP86 functional. Complex **2f** is not included in the graph (see text).

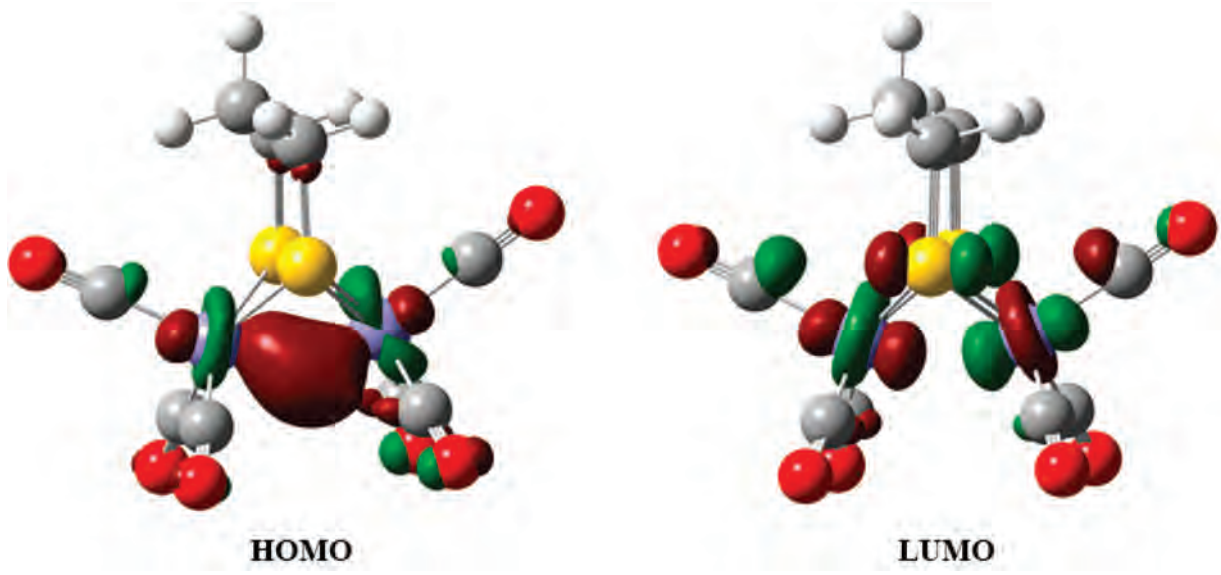

Figure 7. Molecular orbital plot of the HOMO (left) and LUMO (right) for complex **1a**.

Table 4. Mulliken 3d Population of the Neutral Species in Gas Phase

complex	Fe1	Fe2	total	E_{calc}/V
1a	7.117	7.067	14.183	−1.59
2a-Ba1	7.105	7.116	14.221	−1.90
2b	7.172	7.109	14.281	−1.83
2c	7.192	7.111	14.302	−1.95
2d-Ba/Ba-cis	7.100	7.105	14.206	−2.15
2e	7.165	7.172	14.337	−2.22

Presumably, the calculated one-electron redox potentials should correlate with the HOMO and LUMO energies of the Fe^IFe^I complexes as well as the SOMO of the oxidized/reduced species. Shown in Figure 6 is a plot of the gas phase Fe^IFe^I HOMO/LUMO energies for the BP86 calculations versus the calculated oxidation/reduction potential, respectively, including linear regression analysis. Complex **2f** is not included because molecular ions that bear substantial negative charges exhibit unrealistic HOMO/LUMO energies when not surrounded by counterions.[77]

The R^2 values for the quality of fit is 0.874 (0.951) for the HOMO (LUMO) energies of the Fe^IFe^I species. A high correlation constant (~0.93) also exists between the SOMO energies of the $Fe^{II}Fe^I/Fe^IFe^0$ versus oxidation/reduction potentials, respectively. Both show excellent agreement between the orbital energies versus redox potentials, suggesting that one could eliminate the amount of computational effort required to conduct *in vacuo* geometry optimizations and SCRF calculations for cationic, neutral, and anionic species. A linear relationship expressing the HOMO/LUMO orbital energy, $E_{Fe^IFe^IMO}$, of the Fe^IFe^I species in eV and the predicted one-electron oxidation/reduction potential, E_{Pred}, in V is shown in eq 7:

$$E_{Pred} = aE_{Fe^IFe^IMO} - b \qquad (7)$$

The constants a and b are derived from the data and can be found in Table 3. This equation is based on acetonitrile as the solvent and ferrocene as the standard. Assuming future complexes follow the same redox chemistry, one can then easily predict the reduction potential of a proposed compound from a single *in vacuo* geometry optimization calculation to within ±0.13 V (±0.07 V) for oxidation (reduction).

Figure 7 shows the HOMO and LUMO molecular orbital plots for **1a**, which is representative of all compounds studied. The HOMO is characterized by a metal−metal bond symmetrically distributed among the iron centers, and the LUMO is best described as the metal−metal antibonding orbital.[23,78]

Considering the effects of the ligands on observed redox properties, one would expect that the electron density on the Fe center should increase according to the spectrochemical series

$$CO > CNCH_3 > CN- > PPh_3 > PPh(CH_3)_2 \qquad (8)$$

as CO is replaced by ligands that are better sigma donors and poorer pi acceptors. These substitutions should make the complex easier to oxidize and more difficult to reduce, thereby lowering the potential. These trends are in fact observed both in the calculations and the experiments with two exceptions. The cyanide analogue does not follow the trend because of its dianionic charge, and for the case of monosubstituted methylisocyanide ($CNCH_3$) analogue the calculated redox potentials is only slightly lower than triphenylphosphine. One possible error in the reduction of the monosubstituted methylisocyanide derivative could be the inability to predict a correct geometry for the anion, since cyclic voltammetry experiments show that the compound has an irreversible reduction.[21] While these trends are intuitive to the average inorganic chemist, it is particularly interesting that they are maintained especially since these reductions are not necessarily reversible on the electrochemical time scale.

The increase in electron density on the metal is also borne out by the calculations as CO is replaced by other ligands in the series. Albeit small, there is some amount of ligand character found in the LUMO which could explain the trend in donating ligand versus reduction potential. We can trace

the reduction potential to the Mulliken 3d population of each Fe in the neutral species using the pdt bridging ligand, shown in Table 4. Although total atomic charges using Mulliken analysis are often counter-intuitive in these calculations, it is our experience with molecular systems that the individual net d and f populations in transition metal and lanthanides/actinides are generally compatible with chemical intuition. Note that Fe_1 is the proximal iron atom to the β carbon of the $S_2C_3H_6$ ligand and Fe_2 is the distal metal center (see Scheme 2). Upon coordination of the more donating ligands, the weak σ^* interaction between the Fe^IFe^I destabilizes the LUMO, and the Mulliken 3d population on proximal Fe increases when moving across the series. The destabilization is then reflected in the reduction potential. The only discrepancy occurs in the mono- and disubstituted isocyanide complexes (**2a** and **2d**), where the Fe Mulliken 3d populations do not appreciably change from the all carbonyl complex of **1a**. Because the lowest energy isomers in these complexes consist of a basal configuration of the isocyanide ligands, we would not expect that the donating ability of the methylisocyanide ligands to affect the d population. However, the reduction potential of these complexes is lowered because the ligand is reduced; the methylisocyanide ligand angle changes by 40° upon reduction of the compound.

Conclusions

One-electron redox potentials have been calculated for a series of dinuclear Fe^IFe^I model complexes mimicking the active site of [FeFe]H_2ase and are in excellent agreement with experiment when using the uBP86 functional. Calculations using uB3LYP functional reproduce the trend but require a consistent shift of −0.82 and −0.53 V to compare the oxidation and reduction potentials, respectively, to experiment. We examined the bonding and d-electron populations of the Fe ions to rationalize the calculated and observed reduction potentials. The redox potential correlates well to the spectrochemical series for the ligands studied and can be justified by the amount of electron density donated by the ligand onto the Fe centers.

Acknowledgment. This work was supported by the Laboratory Directed Research and Development (LDRD) program at Los Alamos National Laboratory. Los Alamos National Laboratory is operated by Los Alamos National Security, LLC, for the National Nuclear Security Administration of the U.S. Department of Energy under contract DE-AC52-06NA25396.

Supporting Information Available: Selected experimental and computed bond distances for compounds with corresponding X-ray crystallographic data; experimental and computed ν(CO) and ν(CN) frequencies (cm^{-1}) for all compounds; optimized structures and selected bond lengths (Å) for complex **2a** and **2d** using the BP86 functional; calculated IR spectra of **2a** and **2d** isomers using the BP86 functional in the gas phase; optimized structures and selected bond lengths (Å) for the reduced and oxidized complexes **1a**−**2f** using the BP86 functional; calculated IR spectrum of [**1a**]$^-$ and [**1b**]$^-$ isomers using the BP86 functional; gas phase electron attachment and ionization energies (kcal mol^{-1}) including ZPE, thermal enthalpic, and entropic corrections; SOMO energies/eV of the $Fe^{II}Fe^I$ and Fe^0Fe^I complexes, respectively, versus the calculated redox potentials, E_{calc}/V, using the BP86 functional. This material is available free of charge via the Internet at http://pubs.acs.org.

IC800541W

(77) Roy, L. E.; Hughbanks, T. *Inorg. Chem.* **2006**, *45*, 8273–8282.
(78) Dahl, L. F.; Wei, C.-H. *Inorg. Chem.* **1963**, *2*, 328–333.